Lawrence Berkeley National Laboratory

Title
Spatio-Temporal Convergence of Maximum Daily Light-Use Efficiency Based on Radiation Absorption by Canopy Chlorophyll

Permalink
https://escholarship.org/uc/item/4xr425x5

Authors
Zhang, Yao
Xiao, Xiangming
Wolf, Sebastian
et al.

Spatio-Temporal Convergence of Maximum Daily Light-Use Efficiency Based on Radiation Absorption by Canopy Chlorophyll

Yao Zhang[1,2], Xiangming Xiao[1,3], Sebastian Wolf[4], Jin Wu[5], Xiaocui Wu[1], Beniamino Gioli[6], Georg Wohlfahrt[7], Alessandro Cescatti[8], Christiaan van der Tol[9], Sha Zhou[10], Christopher M. Gough[11], Pierre Gentine[2], Yongguang Zhang[12], Rainer Steinbrecher[13], and Jonas Ardö[14]

[1] Department of Microbiology and Plant Biology, Center for Spatial Analysis, University of Oklahoma, Norman, OK, USA, [2] Department of Earth and Environmental Engineering, Columbia University, New York, NY, USA, [3] Ministry of Education Key Laboratory of Biodiversity Science and Ecological Engineering, Institute of Biodiversity Science, Fudan University, Shanghai, China, [4] Department of Environmental Systems Science, ETH Zurich, Zurich, Switzerland, [5] Biological, Environmental and Climate Sciences Department, Brookhaven National Lab, Upton, NY, USA, [6] Institute of Biometeorology, National Research Council, Florence, Italy, [7] Institute of Ecology, University of Innsbruck, Innsbruck, Austria, [8] Directorate for Sustainable Resources, Joint Research Centre, European Commission, Ispra, Italy, [9] Department of Water Resources, Faculty ITC, University of Twente, Enschede, Netherlands, [10] State Key Laboratory of Hydroscience and Engineering, Department of Hydraulic Engineering, Tsinghua University, Beijing, China, [11] Department of Biology, Virginia Commonwealth University, Richmond, VA, USA, [12] Jiangsu Center for Collaborative Innovation in Geographical Information Resource Development and Application, International Institute for Earth System Sciences, Nanjing University, Nanjing, China, [13] Department of Atmospheric Environmental Research, Institute for Meteorology and Climate Research, Karlsruhe Institute of Technology, Garmisch-Partenkirchen, Germany, [14] Physical Geography and Ecosystem Science, Lund University, Lund, Sweden

Correspondence to: Y. Zhang and X. Xiao, yaozhang@ou.edu; xiangming.xiao@ou.edu

Abstract

Light-use efficiency (LUE), which quantifies the plants' efficiency in utilizing solar radiation for photosynthetic carbon fixation, is an important factor for gross primary production estimation. Here we use satellite-based solar-induced chlorophyll fluorescence as a proxy for photosynthetically active radiation absorbed by chlorophyll ($APAR_{chl}$) and derive an estimation of the fraction of $APAR_{chl}$ ($fPAR_{chl}$) from four remotely sensed vegetation indicators. By comparing maximum LUE estimated at different scales from 127 eddy flux sites, we found that the maximum daily LUE based on PAR absorption by canopy chlorophyll (ε_{max}^{chl}), unlike other expressions of LUE, tends to converge across biome types. The photosynthetic seasonality in tropical forests can also be tracked by the change of $fPAR_{chl}$, suggesting the corresponding ε_{max}^{chl} to have less seasonal variation. This spatio-temporal convergence of LUE derived from $fPAR_{chl}$ can be used to build simple but robust gross primary production models and to better constrain process-based models.

Plain Language Summary

Plants absorb light to fix carbon dioxide; the efficiency of this process is termed as light-use efficiency and can be calculated based on different light absorption definitions. Among the light being absorbed by plants, only a fraction is captured by chlorophyll and can be further used for

photosynthesis. In this study, we used satellite data and derived an estimation of the fraction of light that is absorbed by chlorophyll. We found that different plants have a similar efficiency using chlorophyll-absorbed light to fix carbon dioxide; this efficiency is also found to be stable throughout the season in tropical forest. The results of this study can be used to improve models' capability to estimate the total carbon fixed by plants at global scale.

1 Introduction

Plants fix carbon through photosynthesis, sequestering carbon dioxide from the atmosphere and substantially mitigating the negative impact of anthropogenic CO_2 emissions on climate. Carbon cycle studies often quantify photosynthesis at local, regional, and global scales as gross primary productivity (GPP), the quantity of carbon fixed prior to losses from respiration. Many approaches are available to estimate GPP at different temporal and spatial scales, including in situ observations from leaf-level chamber measurements of gas exchange and ecosystem-level eddy covariance (EC) technique (Baldocchi et al., 2001), and model estimation using indirect remote sensing observations or ecological models at regional and global scales (Alemohammad et al., 2017; Anav et al., 2015; Running et al., 2004).

The production efficiency model (PEM) or light-use efficiency (LUE) model offers a very simple and broadly applied conceptual framework to estimate GPP at different spatial scales (Monteith, 1972). This class of models calculates GPP using the product of the photosynthetically active radiation (PAR), the fraction of absorbed PAR (fPAR), and a LUE factor, which converts energy absorbed into the amount of carbon fixed:

$$GPP = PAR \times fPAR \times LUE \ (1)$$

LUE is often calculated as a function of the maximum daily LUE (ε_{max}) regulated by environmental controls (temperature, soil water, vapor pressure deficit, etc.). The variation of LUE can be large, while ε_{max} is often regarded as a constant parameter for each biome type in most LUE models. The product of the first two terms on the right-hand side in equation 1 is absorbed PAR (APAR = PAR × fPAR), which can be expressed variously as incident PAR (fPAR = 1), PAR absorbed by the entire (nonphotosynthetic and photosynthetic) canopy ($fPAR_{canopy}$) or by chlorophyll in all leaves of the canopy ($fPAR_{chl}$, photosynthetic-only; Figure S1). Because of the different definitions of APAR, the LUE factor in equation 1, which corresponds to different ε_{max} values, can differ substantially. In most studies, ε_{max} is an empirical parameter estimated from equation 1 that varies greatly because of the different LUE definitions (Song et al., 2013). Therefore, ε_{max} values cannot be used/compared when they are derived from different fPAR bases.

Most PEMs employ the PAR absorbed by vegetation canopy ($APAR_{canopy}$) to estimate GPP (GPP = LUE_{canopy} × $APAR_{canopy}$), for example, the Carnegie-Ames-

Stanford Approach model (Potter et al., 1993) and the Moderate Resolution Imaging Spectroradiometer (MODIS) GPP algorithm (Running et al., 2004), where the fPAR is typically calculated as a function of satellite-derived normalized difference vegetation indices (NDVIs) or leaf area index (LAI). However, not all light absorbed by the canopy is used in the photosynthetic process (Figure S1). A substantial fraction of PAR will be absorbed by the nonphotosynthetic vegetation (NPV, e.g., branch, stem, dry leaf, nonphotosynthetic pigments, and materials; Xiao et al., 2004). Importantly, the fraction of NPV is different across different biomes (Li & Guo, 2016). As a result, in those PEM models, ε_{max} may be biome-specific as $APAR_{canopy}$ is not corrected for the fraction of PAR absorbed by NPV (McCallum et al., 2009; Potter et al., 1993). However, the variation of NPV ratio within biomes is not considered in these models. In addition, the NPV composition also varies with vegetation phenology and growth over seasons and years (Guerschman et al., 2009). Thus, there is a need to account for the temporal variability of biotic factors such as changes in the fraction of chlorophyll/NPV with phenological cycles.

One fundamental theoretical assumption is that with more precise representation of fPAR absorbed by chlorophyll, estimates of ecosystem GPP are significantly improved by reducing bias and variability associated with unaccounted differences among biomes or across time in the ratio of chlorophyll to NPV. If GPP is more tightly coupled with chlorophyll-absorbed PAR as hypothesized, the range of ε_{max} variations across space and time will be smaller when estimated from the absorbed energy by chlorophyll, which is used to drive photosynthesis. Previous studies have shown that the LUE is more stable across the seasonal cycle in a cropland when using radiation absorption by chlorophyll than by leaf or canopy (Gitelson & Gamon, 2015; Peng et al., 2011). However, these studies focused on a single vegetation type and used data at a single site. Whether this phenomenon can be extrapolated to other biome types at seasonal scale or across different biome types remains unclear.

Successful retrievals of solar-induced chlorophyll fluorescence (SIF) from satellites (Frankenberg et al., 2011; Joiner et al., 2013) provide a new probe of vegetation photosynthesis at regional to global scales (Porcar-Castell et al., 2014). SIF is a very small fraction (~1–2%) of energy reemitted during the light reactions of photosynthesis. Photons absorbed by excited chlorophyll have three pathways: photochemical quenching (used for photosynthesis), nonphotochemical quenching (heat dissipation), and fluorescence (Genty et al., 1989; Figure S1). Because SIF is only emitted from photosystems and can be interpreted as the photosynthetic electron transport rate under unstressed condition (Zhang et al., 2014), it can be a good proxy of PAR absorbed by the chlorophyll ($APAR_{chl}$) that is more precisely focused on photosynthetic pigments than traditional measures of ecosystem or canopy APAR (Zhang, Xiao, Jin, et al., 2016). However, current long-term SIF observations have relatively high uncertainties and low spatial

resolution (Joiner et al., 2014), which complicates direct comparisons with EC flux tower observations of LUE and GPP. Most PEMs still use satellite-based optical vegetation activity indicators (OVAIs; Table S1; Elsobky, 2015; Yan et al., 2016) to estimate as $fPAR_{canopy}$ or $fPAR_{chl}$, which allow GPP simulation at spatial resolutions comparable to the footprint of EC flux tower sites.

In this study, we try to test our hypothesis that the maximum daily LUE based on radiation absorbed by chlorophyll (ε_{max}^{chl}, corresponding to LUE_{chl} and $APAR_{chl}$) is more stable than other ε_{max} definitions in space and time. This hypothesis, if verified, would help us to build new PEM without biome-specific parameterizations of ε_{max}. To test this hypothesis, we followed these three steps:

1. We first derive proxies of $fPAR_{chl}$ and $fPAR_{canopy}$ from OVAIs so that they can be directly compared with GPP and PAR from flux towers. To do this, we explore the relationship between SIF and OVAIs upscaled to SIF spatial resolution and estimate $fPAR_{chl}$ from OVAIs (Figure S2). The OVAIs used in this study are satellite-retrieved vegetation indicators such as NDVI, enhanced vegetation index (EVI; Huete et al., 2002), and an fPAR product ($fPAR_{mod15}$; Myneni et al., 2002) from the MODIS as well as the Medium Resolution Imaging Spectrometer terrestrial chlorophyll index (MTCI) from the Medium Resolution Imaging Spectrometer (Dash & Curran, 2004). Through this comparison, we would like to (a) identify which OVAI can serve as better proxies of $fPAR_{chl}$ and (b) build linear relationships between OVAIs and $fPAR_{chl}$.

2. After we obtain the proxies of $fPAR_{chl}$, $fPAR_{canopy}$, and GPP estimated from the FLUXNET data set (Baldocchi et al., 2001), we then calculate ε_{max} for different biomes using different APAR definitions. A spatial convergence of ε_{max}^{chl} would be represented as a more stable relationship between GPP/PAR (LUE_{eco}) and linear proxies of $fPAR_{chl}$ across different biomes over space.

3. To test the temporal convergence, we obtained the reference LUE (LUE_{ref}) from two tropical rainforest sites where LUE under a fixed environment condition can be derived for each month to represent the seasonal variation of ε_{max}. In this way, we can compare the ecosystem LUE without considering the environmental limitations (Figure S2). A temporal convergence of ε_{max}^{chl} would be represented as $fPAR_{chl}$ fully tracking the monthly variations in LUE_{ref}.

2 Materials and Methods

2.1 Solar-Induced Chlorophyll Fluorescence as a Proxy of $APAR_{chl}$

The SIF product for the period from 2007 to 2015 was retrieved from the Global Ozone Monitoring Experiment 2 (GOME-2) instrument onboard the MetOp-A satellite (Joiner et al., 2013). The GOME-2 V27 SIF product used in this study has a spatial resolution of 0.5° × 0.5° and monthly temporal

resolution. SIF can be expressed using a similar form to the LUE models (Guanter et al., 2014; Joiner et al., 2014):

$$SIF = PAR \times fPAR_{chl} \times FE \quad (2)$$

where FE is the fluorescence efficiency observed at top of canopy. Because SIF retrieved from GOME-2 is a snapshot of vegetation activity in space and time, we use the cosine of the Sun zenith angle (SZA) to approximate the instantaneous PAR when the satellite observation is made:

$$PAR = \beta \times \cos(SZA) \quad (3)$$

where β is the solar constant, representing sea-surface clear-sky solar radiation when the Sun is at the zenith, that is, $\cos(SZA) = 1$. Thus, equation 2 can be written in a different form:

$$fPAR_{chl} = \frac{SIF}{\beta \times \cos(SZA) \times FE} \quad (4)$$

Previous studies also showed that SIF is mostly driven by the amount of radiation absorbed by chlorophyll under unstressed conditions (Liu et al., 2017; Yang et al., 2015). Simulations using the Soil Canopy Observation of Photochemistry and Energy fluxes (SCOPE) model suggest that FE is relatively stable using various parameter combinations. A detailed description of this analysis can be found in the supporting information Text S1 and Figures S3 and S4 (van der Tol, Verhoef, & Rosema, 2009; van der Tol, Verhoef, Timmermans, et al., 2009; Verhoef, 1984, 2011; Verrelst et al., 2015; Zhang et al., 2014). Although drought and other environmental stresses also affect FE, this effect is limited because of the averaging of the SIF signal in the spatial and temporal domain. In addition, the energy partitioning through heat dissipation for light-adapted conditions (ϕ_N) is limited and has less effect on FE at 9:30 a.m. (GOME-2 overpass time) than midday (Amoros-Lopez et al., 2008). Only prolonged and severe drought that directly affect the heat dissipation for dark-adapted conditions (ϕ_D) will decrease FE (Adams & Demmig-Adams, 2004; Baker, 2008). Therefore, we regard FE as a constant in this study and the uncertainties are considered in the error propagation analysis (Text S3). With this approximation, we define $fPAR_{SIF}$ as $SIF/\cos(SZA)$; considering a constant β and FE in equation 4, $fPAR_{SIF}$ is proportionate to $fPAR_{chl}$:

$$fPAR_{chl} \propto fPAR_{SIF} = \frac{SIF}{\cos(SZA)} \quad (5)$$

where $fPAR_{SIF}$ does not follow the conventional range of 0 to 1, but that of an empirical parameter that can be calculated from SIF data. We use this relationship to evaluate proxies for $fPAR_{chl}$ using OVAIs both temporally for each pixel and spatially for each month.

Because of the linear form of PEMs (equation 1), we use a linear transformation of OVAIs to approximate $fPAR_{chl}$ as follows:

$$fPAR_{chl} = a \times (OVAIs - c) \propto fPAR_{SIF} \quad (6)$$

The slope (a) can be regarded as a part of LUE and ideally, should be a fixed number for all biome types. The intercept (c) can be estimated from the intercept of the regression. A relatively stable regression slope and intercept between OVAIs and $fPAR_{SIF}$ both spatially and temporally indicates that the approximation in equation 6 is plausible. The values ($OVAIs - c$) are considered as a proxy of (or proportional to) $fPAR_{chl}$ and are denoted with a subscripts m (e.g., $EVI_m = EVI - c$). Prior to these regression analysis, OVAIs were subject to a quality check and only good observations were used (supporting information, Text S2; Myneni et al., 2015; Vermote, 2015; Viovy et al., 1992).

2.2 FLUXNET Data Processing and Light-Use Efficiency Calculation

The GPP estimation used in this study is derived from EC data available from the FLUXNET2015 Tier 2 data set (http://fluxnet.fluxdata.org/data/fluxnet2015-dataset/; 2015 December Release; Table S2) processed according to standardized protocols (Pastorello et al., 2017). Out of the 136 available sites we chose 127 sites (or specific site-years for rotated cropland) where C_3 species are dominant. These flux sites cover a variety of ecosystem types, and there are altogether 626 site-years (Table S2 and Figure S5). The daily FLUXNET2015 data sets were aggregated into 8-day intervals (and 10-day intervals for 2008–2012 to compare with MTCI; see section 2.3) after a rigorous data quality check (Text S2).

Limitations of water, temperature, and other climate factors will down-regulate the LUE from its maximum value (ε_{max}). These limitations are complex and vary across ecosystems so that we cannot directly estimate ε_{max} based on GPP and APAR measurements (Zhang, Xiao, Zhou, et al., 2016). In this study, we simplify this issue by assuming (1) that plants in all ecosystems reach their maximum LUE during the peak growing season because of their long-term acclimation of the photosynthetic apparatus given that no severe disturbances occur. This allows us to calculate the maximum ecosystem LUE (ε_{max}^{eco}, corresponds to LUE_{eco} and fPAR = 1) for each site; (2) for tropical rainforest ecosystems, where photosynthesis is active all year round, we followed previous studies (Wu et al., 2016) and used the reference LUE (LUE_{ref}) as the seasonal variation of ε_{max}^{eco}. LUE_{ref} is calculated as ecosystem LUE (LUE_{eco} = GPP/PAR) under a small range of climate conditions (e.g., cloudiness, PAR, air temperature, and vapor pressure deficit) within each month throughout the year, so that the effect of environmental limitations on photosynthesis is constant and can be eliminated.

For each site-year, we identified the five 8-day (four 10-day) period with the highest GPP values as the peak growing season. For each 8-day (10-day) period during the peak growing season, ε_{max}^{eco} was then calculated as the average of daily GPP from EC measurements (GPP_{EC}) divided by the average of daily PAR. However, as disturbances may occur in some years and climate

may limit LUE during the peak growing season, we only retained the upper 50th percentile of ε_{max}^{eco} from all available years for each site for further analysis.

As several studies have shown that ε_{max} varies between clear and cloudy days (Mercado et al., 2009), we separate the sunny and cloudy period for each 8-day (10-day) period during the peak growing season using a clearness index (actual shortwave radiation/top of atmosphere shortwave radiation) of 0.55 (which is ~80% of its maximum actual value because of atmospheric scattering). Corresponding to the different definitions of fPAR (Figure S1), ε_{max} can also be calculated at different levels, using incoming PAR (ε_{max}^{eco} = GPP$_{EC}$/PAR), canopy-absorbed PAR ($\varepsilon_{max}^{canopy}$ = GPP$_{EC}$/APAR$_{canopy}$), and chlorophyll-absorbed PAR (ε_{max}^{chl} = GPP$_{EC}$/APAR$_{chl}$) during the peak growing season when there is no environmental limitation (Gitelson & Gamon, 2015; Zhang et al., 2009). For $\varepsilon_{max}^{canopy}$ and ε_{max}^{chl}, they can also be calculated from ε_{max}^{eco}/fPAR$_{canopy}$ and ε_{max}^{eco}/fPAR$_{chl}$, respectively. Therefore, a convergence of ε_{max} from canopy to chlorophyll level across biome types will be represented as a convergence of regression slopes in the linear regression (with 0 intercept) between LUE$_{eco}$ and fPAR$_{chl}$ compared to LUE$_{eco}$ and fPAR$_{canopy}$.

2.3 Remote Sensing Observations at Flux Tower Sites

We used two vegetation indices (NDVI and EVI), one fPAR product (fPAR$_{mod15}$) from MODIS and one chlorophyll index (MTCI) to represent the fPAR$_{canopy}$ and their transformations (OVAIs−c) as proxies of fPAR$_{chl}$ (Table S3). Due to the sensitivity of remote sensing retrievals to atmospheric contaminations, when comparing the remotely sensed OVAIs with eddy flux measurements, we used a similar procedure reported in Zhang, Xiao, Zhou, et al. (2016) to screen and gap-fill the remotely sensed OVAI observations of poor quality (see details in supporting information, Text S2). Considering the multiple approximations in the previous steps and the uncertainty in each data set, an error propagation analysis, described in supporting information Text S3 (Deming, 1943), was performed.

To reduce artifacts caused by Sun-sensor geometry or bi-directional reflectance distribution function (BRDF), we used the Multi-Angle Implementation of Atmospheric Correction (MAIAC) algorithm reflectance data set (Lyapustin et al., 2012) to calculate NDVI and EVI for the Amazon K67 (2.85°S, 54.97°W) and K34 (2.61°S, 60.21°W) sites. The MAIAC algorithm implements rigorous BRDF and atmospheric corrections and is therefore more robust than EVI calculated from MOD09A1 C6 when detecting changes in tropical forests (Hilker et al., 2014). We retrieved the reflectance for the nine surrounding pixels (3 km by 3 km) for sites K67 and K34 from 2000 to 2012 and then calculated the NDVI and EVI using the BRDF corrected reflectance.

3 Results

3.1 Relationship Between fPAR$_{SIF}$ and OVAIs

We calculated the averages of OVAIs for all pixels within each vegetation type for each month and compared them with fPAR$_{SIF}$ for the period 2007 to 2015 (2007 to 2012 for MTCI). For fPAR$_{mod15}$ and NDVI, their relationships with fPAR$_{SIF}$ for different biome types were scattered, and the R^2 of the regression within each biome type was relatively lower compared to those for EVI and MTCI (Figure 1). EVI and MTCI also showed a stronger linear correlation with fPAR$_{SIF}$ when all the biome types were combined together. The relationship between fPAR$_{SIF}$ and MTCI was also consistent across biomes.
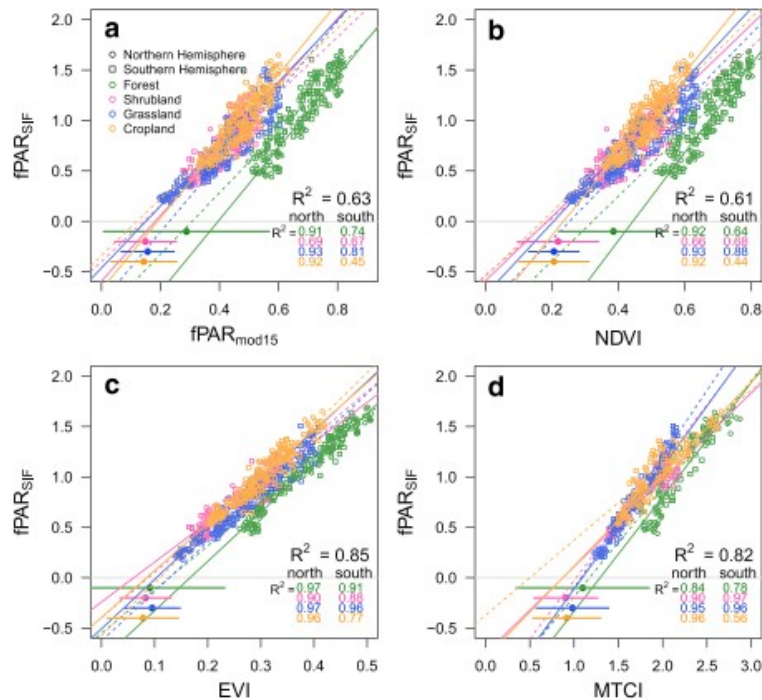
Figure 1. Relationships between fPAR$_{SIF}$ and four optical vegetation activity indicators. Each point represents the average value of all the gridcells within a specific land cover type for either the northern or southern hemisphere for each month. Land cover types were aggregated from Moderate Resolution Imaging Spectroradiometer land cover map (Text S4 and Figure S10). Two hemispheres were calculated separately because of different phenological cycles. The solid lines represent regressions for the northern hemisphere, and the dashed lines represent regressions for the southern hemisphere. The coefficients of determination for each regression are given in the lower-right corner. The four horizontal lines with dots below fPAR$_{SIF}$ = 0 (lower left corner) represent the mean value and standard deviation of the regression intercepts between the fPAR$_{SIF}$ and optical vegetation activity indicators in the temporal domain for individual pixel grouped by different land cover types (Figure S6; Friedl et al., 2010).

The intercepts of these linear regressions (c in equation 6) are important to establish and assess variations in the relationship between OVAIs and fPAR$_{chl}$. We compared the intercept estimates from both the spatially averaged regressions (Figure 1) and the regressions of individual gridcells (Figure S6). MTCI and EVI showed less variable intercepts than fPAR$_{mod15}$ and NDVI across four biome types. The fPAR$_{mod15}$ and NDVI exhibited a larger variation of intercepts than that of EVI and MTCI when different biome types were considered.

We also used simple linear regression to determine the relationship between monthly fPAR$_{SIF}$ and OVAIs for individual gridcell. Figure 2 shows the spatial pattern and the frequency statistics of the regression slopes between

fPAR$_{SIF}$ and the four OVAIs with fixed intercepts from the previous steps. The spatial variations of the regression slopes using fPAR$_{mod15}$ and NDVI were relatively larger than those using EVI and MTCI, as represented by larger coefficients of variation. The frequency statistics of these regression slopes showed biome-specific characteristics for fPAR$_{mod15}$, NDVI, and EVI, where the lowest values were found for forests, followed by shrublands, grasslands, and croplands. The MTCI, on the other hand, showed a relatively stable slope across the different biome types. In addition, EVI also showed slightly higher coefficients of determination (R^2) for the regression models (Figure S7). Based on these analyses, EVI and MTCI were considered stronger proxies of fPAR$_{chl}$ than either fPAR$_{mod15}$ or NDVI. The average intercepts on the x axis were ~0.1 for EVI and ~1.0 for MTCI. We used these intercepts to build the relationship between OVAIs and the fPAR$_{chl}$.
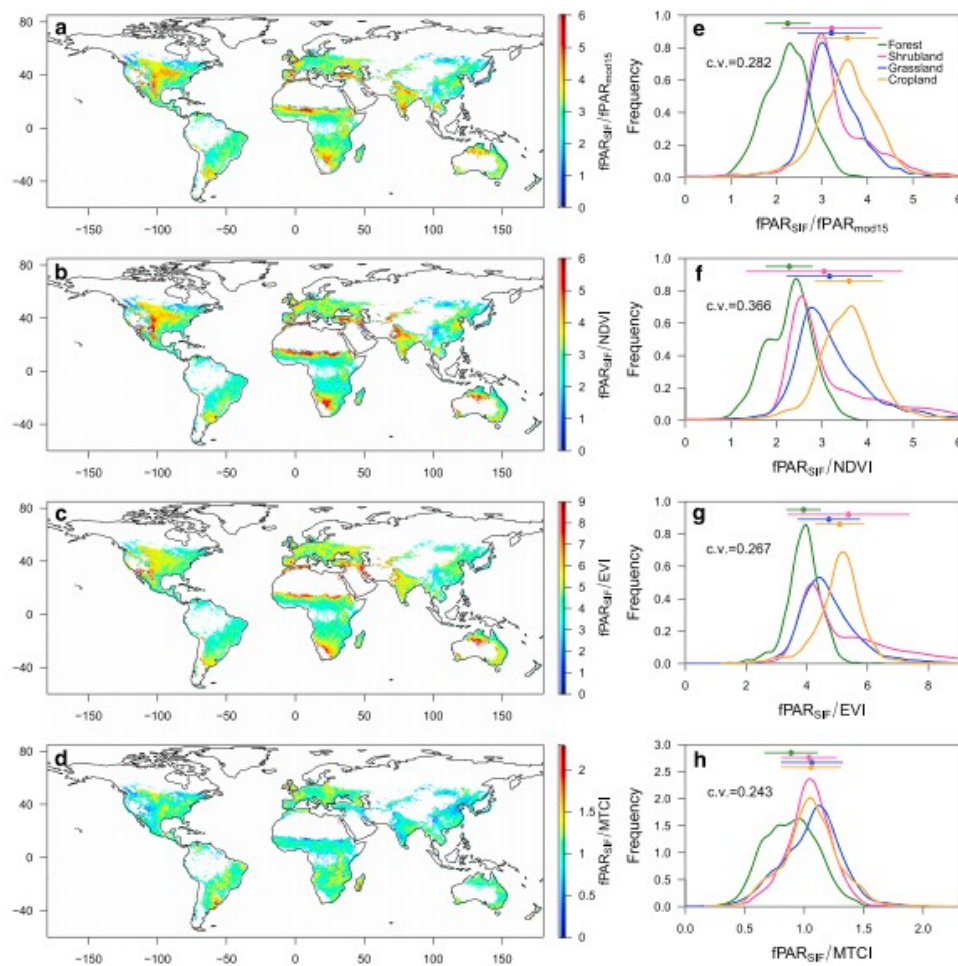
Figure 2. Spatial distribution and frequency distribution of the regression slopes between fPAR$_{SIF}$ and four optical vegetation activity indicators with fixed intercepts (c in equation (6)) for the period 2007 to 2015 (2007–2012 for MTCI). The left column (a–d) shows the spatial distribution of regression slopes where the regression is significant at 0.05 level. The white areas in tropical and boreal region are caused by very limited valid observations after quality check. The right column (e–h) shows the frequency distribution of four major land cover types. Points with error bars at the top of each plot represent the mean ± 1 standard deviation of the slopes within each land cover type.

3.2 Different LUE Estimation Across Biomes Based on Flux Tower GPP

To compare with GPP estimated from flux towers (GPP_{EC}), we used the EVI_m ($EVI_m = EVI - 0.1$), $MTCI_m$ ($MTCI_m = MTCI - 1$), as approximations of $fPAR_{chl}$, and the original $fPAR_{mod15}$ and NDVI with different intercept values as $fPAR_{canopy}$ (Figure S1). For clear days, the regressions between ε_{max}^{eco} and EVI_m or $MTCI_m$, which are considered better $fPAR_{chl}$ approximations, showed a smaller variation of regression slopes within each biome types than those using the other two canopy indicators ($fPAR_{mod15}$ and NDVI; Figures 3a–3d). EVI_m and $MTCI_m$ were also characterized by a smaller root-mean-square errors and higher coefficients of determination (R^2) than fPAR and NDVI when all biome types were combined together (Tables S4 and S5). Similar results were also found for cloudy days (Figures 3e–3h) and when using NDVI with different intercepts as $fPAR_{canopy}$ proxies (Figure S8). From the ecosystem (top of canopy) PAR absorption to canopy or chlorophyll PAR absorption, the corresponding maximum daily LUE converges as shown by smaller coefficients of variation across biomes using fPAR = 1, $fPAR_{canopy}$, and $fPAR_{chl}$ approximations (Figures 3i and 3j).
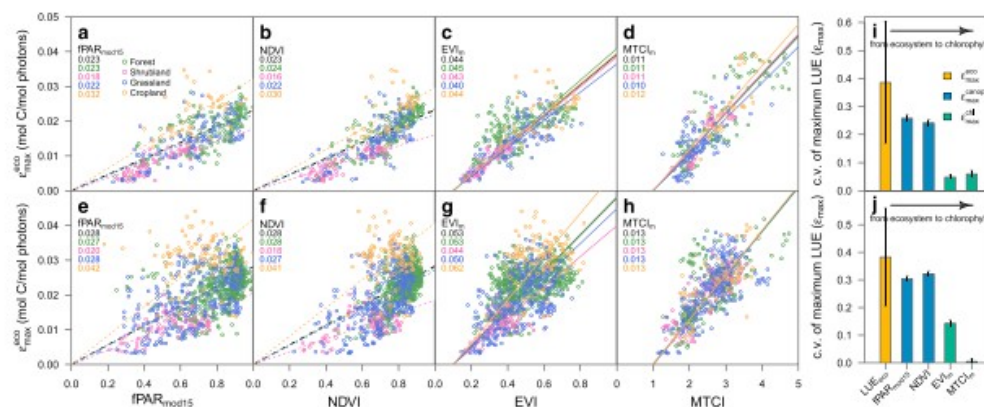

Figure 3. (a–h) Relationship between different OVAIs and LUE_{eco} for peak growing season using GPP_{EC} from clear days (upper panel) and cloudy days (lower panel). Each open circle represents one week from a site year. The solid lines represent the regression between LUE_{eco} and $fPAR_{chl}$ proxies (EVI_m, $MTCI_m$), which are forced to pass [c,0] (c for the fixed intercept in equation (6)); the dashed lines represent the regression between LUE_{eco} and $fPAR_{canopy}$ proxies ($fPAR_{mod15}$ and NDVI), which are forced to pass [0,0]. The numbers in the top left corner of each subplot are the regression slopes representing the $\varepsilon_{max}^{canopy}$ (a, b, e, and f) and ε_{max}^{chl} (c, d, g, and h) for each land cover type (see section 2.2). Regressions lines and slope values (ε_{max}) in black represent all biome types combined together. Summary of ε for different APAR definitions based on regression slopes in (a–h) for clear days (i) and cloudy days (j). The error bar on each bar is calculated from error propagation considering all the uncertainties in both input data sets and each approximation step (supporting information Text S3).

3.3 Using $fPAR_{chl}$ Approximations to Track Seasonal Dynamic of Reference LUE

We also tested whether this convergence can be found across time, that is, whether the seasonal changes of LUE_{ref} can be explained by the change of the canopy chlorophyll. We chose two tropical rainforest sites in the Amazon forest where multiyear eddy flux observations were available (Wu et al., 2016). For both sites, $MTCI_m$ showed a similar seasonal pattern of LUE_{ref}, while NDVI was not sensitive to seasonal changes (Figure 4). This represents that the seasonal variation of ε_{max}^{eco} can be better explained by $fPAR_{chl}$ than

fPAR$_{canopy}$ (NDVI); therefore, the ε_{max}^{chl} (ε_{max}^{eco}/fPAR$_{chl}$) has a smaller variation at seasonal scale compared to $\varepsilon_{max}^{canopy}$.
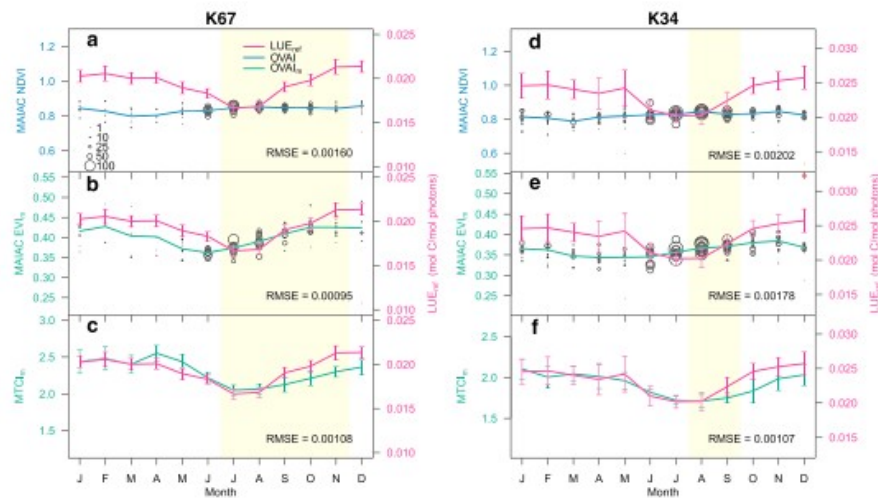

Figure 4. Comparing fPAR$_{canopy}$ (NDVI) and approximation of fPAR$_{chl}$ (EVI$_m$, MTCI$_m$) with LUE$_{ref}$ at (a–c) K67 and (d–f) K34 sites in Amazon forest. EVI and NDVI data are calculated from MAIAC reflectance. Each circle in (a, b, d, and e) represents the average of all valid observations of vegetation indices for each year each month. The size of the circles represents the numbers of valid observations used. Some obvious outliers were colored in red and eliminated from further analysis. The blue and green lines in (a, b, d, and e) represent the observation numbers weighted averages of EVI or NDVI. The error bars for LUE$_{ref}$ represent the standard error of mean. The error bars for MTCI$_m$ in (c and f) represent the standard deviation for the period 2002 to 2012. The shades in light yellow represent dry season. Root-mean-square errors (RMSEs) are calculated based on regressions with zero intercept.

4 Discussion

4.1 Advantages and Biophysical Interpretation of fPAR$_{chl}$

In this study, we show that EVI and MTCI are robust proxies of fPAR$_{chl}$ with the possible uncertainties being taken into consideration; the maximum daily LUE for PAR absorption by chlorophyll (ε_{max}^{chl}) exhibited less variation in space and time than $\varepsilon_{max}^{canopy}$ and ε_{max}^{eco}. One implication is that a fixed ε_{max}^{chl} can be usable for GPP estimation for C$_3$ plant-dominated ecosystems across space and time. Although NDVI and fPAR were also considered to capture the greenness of the canopy when first employed in PEMs, they did not perform as well as other chlorophyll-related indices in estimating canopy photosynthesis (Rossini et al., 2012; Xiao et al., 2004). Using the SIF retrieval from satellite and flux sites across the globe, our study further demonstrated the advantage of these approaches as a more directed proxy of fPAR$_{chl}$. Our study also supports the long-proposed convergence of LUE theory based on the optimization of resource allocation (Field, 1991; Goetz & Prince, 1999). However, the possible explanation for better proxies of fPAR$_{chl}$ using EVI and MTCI may be different. EVI is known to be less prone to saturation under high biomass or LAI conditions (Huete et al., 2002). When leaf quantity keeps increasing under moderate to high LAI, the APAR$_{chl}$ also increases because of the increases in total chlorophyll content in the canopy. EVI, compared to NDVI or fPAR$_{mod15}$, suffers less from saturation and thus shows a higher correlation with fPAR$_{chl}$. MTCI, on the other hand, is a good indicator for canopy chlorophyll content (Dash & Curran, 2004). Therefore, it can be

directly linked to $fPAR_{chl}$ although a saturation effect may exist as well when total chlorophyll content is high (Peng et al., 2011).

Chlorophyll content has been successfully retrieved at canopy scale as the interaction between these pigments and light affects the canopy reflectance spectrum (Asner & Martin, 2008; Curran, 1989). Compared with PEMs which only focus on the LAI or $fPAR_{canopy}$, the use of $fPAR_{chl}$ can better estimate both leaf quantity (LAI) and leaf physiological quality (chlorophyll concentration and nitrogen content), the latter is often regarded as the secondary factor responsible for LUE_{canopy} (Wu et al., 2016). The possible explanation for this spatio-temporal convergence may be that all the C_3 plants share the same electron transport mechanism and chemical reactions to fix carbon. And all plants under different environmental conditions tend to maximize their photosynthetical capacity during the peak growing season to increase their competitiveness. The variation of $fPAR_{chl}$ in both space and time may also be related to the variation of maximum carboxylation rate (V_{cmax}), quantum efficiency (α_q), and LAI (Croft et al., 2016), but still need additional studies.

4.2 Potential of Using SIF and $fPAR_{chl}$ for GPP Estimation and Data Assimilation

As SIF is closely related to the $APAR_{chl}$, both theoretically from model simulations and experimentally using in situ observations (Frankenberg et al., 2011; van der Tol et al., 2014), this relationship, conserved across biomes, can be used to build simple models to directly estimate GPP from SIF and to improve PEMs (Sun et al., 2017). Guanter et al. (2014) explored the feasibility of estimating GPP using SIF for croplands. Many studies suggest that SIF contains not only the information of light absorption but also the LUE information (Yang et al., 2015). However, these studies all used SIF_{yield} ($SIF_{yield} = SIF/APAR_{canopy}$) defined at the canopy scale. At present, we still do not know whether the good relationship between SIF_{yield} and LUE_{canopy} is caused by the variation of canopy chlorophyll content, which is embedded in both SIF_{yield} and LUE_{canopy} (Figure S1), or to what extent satellite-derived SIF_{yield} actually captures environmental stress on plant physiology. Current GOME-2 data set may not be suitable for the detection of this quick response because of its early morning overpass time and the spatial and temporal aggregation required to reduce SIF data uncertainty. However, understanding this underlying mechanism will pave the way to better estimate GPP from SIF.

The estimates of $fPAR_{chl}$ using vegetation indices also provide an alternative opportunity to benchmark state-of-the-art land surface models. Currently, many dynamic global vegetation models use data assimilation techniques, which employ remote sensing-retrieved LAI or fPAR products to improve performance (Demarty et al., 2007). Other studies try to use SIF or MTCI to constrain model output or inversely estimate some key parameters of the photosynthesis processes (Alton, 2017; Zhang et al., 2014). As we have shown that EVI and MTCI can be used as a proxy of $fPAR_{chl}$ and that ε_{max}^{chl}

appears to converge across different biome types, $fPAR_{chl}$ estimated from EVI and MTCI is more directly related to GPP and can be used for data assimilation to improve model performance.

4.3 Implications for PEMs

Due to their simple form, PEMs play an important role in estimating GPP at regional to global scales. However, the parameterization is a critical issue, especially for ε_{max}, which determines the efficiency of plants converting the daily solar energy to biochemical energy, thus directly affecting the magnitude of the GPP estimation. Previous studies have made efforts to correctly estimate the biome-based ε_{max} (Zhao et al., 2005). Some studies even suggest site-level ε_{max} is necessary to improve model accuracy (Kross et al., 2016). However, it is unlikely that outside of flux tower's footprint, we can obtain spatially continuous in situ GPP measurement to estimate ε_{max}. The spatial convergence of ε_{max}^{chl} across biomes justifies that a constant ε_{max} can be applied for simple but robust parameterization of PEMs. This approach could simplify the model parameterizations by avoiding the need of vegetation maps (e.g., forest, shrub, and grass) and vegetation-specific parameters, ultimately reducing the uncertainty and improving the robustness of the GPP estimates. A new global GPP product from the Vegetation Photosynthesis Model has been developed based on this theory and showed good performance (Zhang et al., 2017). The seasonal dynamics of $fPAR_{chl}$ are closely related to that of LUE_{ref}; however, these biotic changes (LAI and chlorophyll content) are not well represented in $fPAR_{canopy}$-based PEMs. Using $fPAR_{chl}$ could improve the prediction of biotic regulation of GPP at seasonal scale.

Although the cross-biome variation in ε_{max}^{chl} diminishes when using EVI_m and $MTCI_m$ as an approximation of $fPAR_{chl}$, we show that the within-biome ε_{max}^{chl} variation does not decrease much compared to the $fPAR_{canopy}$-based indicators. This may be caused by several reasons: (1) ε_{max}^{chl} is still constrained by environmental conditions and may change from one year to the other year for a given site, even during the peak growing season; (2) site-specific characteristics (soil type, fertilization, etc.) still affect the ε_{max}^{chl} to some extent; (3) the direct and diffuse radiation composition and canopy structure, for example, clumping index, affect ε_{max}^{chl}; (4) flux and satellite measurement uncertainties still exist; and (5) the inconsistency of flux tower footprint and OVAI pixels may introduce noise in the relationship.

5 Conclusions

In this study, we find that based on light absorption by chlorophyll of the canopy, which directly reflects light harvesting of the photosynthesis process, ε_{max}^{chl} tends to converge across space and time, which can greatly simplify the structure and parameterization of PEMs. However, to improve model accuracy, more studies are needed to investigate the environmental limitations on ε_{max} and photosynthesis. Different forms of temperature and

water limitations have been widely used, but recent studies also suggest the need to employ mixed forms of the limitations for forests and nonforested sites, especially during drought periods. With more data accumulated from global flux networks and Earth observation data from different satellites, PEMs will provide more accurate estimates of GPP to support a better understanding of the global carbon cycle.

Acknowledgments

References

Adams, W. W., & Demmig-Adams, B. (2004). Chlorophyll fluorescence as a tool to monitor plant response to the environment. In *Chlorophyll a Fluorescence, Advances in Photosynthesis and Respiration* (pp. 583– 604). Dordrecht: Springer. https://doi.org/10.1007/978-1-4020-3218-9_22

Alemohammad, S. H., Fang, B., Konings, A. G., Aires, F., Green, J. K., Kolassa, J., et al. (2017). Water, Energy, and Carbon with Artificial Neural Networks (WECANN): A statistically based estimate of global surface turbulent fluxes and gross primary productivity using solar-induced

fluorescence. *Biogeosciences*, 14(18), 4101– 4124. https://doi.org/10.5194/bg-14-4101-2017

Alton, P. B. (2017). Retrieval of seasonal Rubisco-limited photosynthetic capacity at global FLUXNET sites from hyperspectral satellite remote sensing: Impact on carbon modelling. *Agricultural and Forest Meteorology*, 232, 74– 88. https://doi.org/10.1016/j.agrformet.2016.08.001

Amoros-Lopez, J., Gomez-Chova, L., Vila-Frances, J., Alonso, L., Calpe, J., Moreno, J., & del Valle-Tascon, S. (2008). Evaluation of remote sensing of vegetation fluorescence by the analysis of diurnal cycles. *International Journal of Remote Sensing*, 29(17-18), 5423– 5436. https://doi.org/10.1080/01431160802036391

Anav, A., Friedlingstein, P., Beer, C., Ciais, P., Harper, A., Jones, C., et al. (2015). Spatiotemporal patterns of terrestrial gross primary production: A review. *Reviews of Geophysics*, 53(3), 785– 818. https://doi.org/10.1002/2015RG000483

Asner, G. P., & Martin, R. E. (2008). Spectral and chemical analysis of tropical forests: Scaling from leaf to canopy levels. *Remote Sensing of Environment*, 112(10), 3958– 3970. https://doi.org/10.1016/j.rse.2008.07.003

Baker, N. R. (2008). Chlorophyll fluorescence: A probe of photosynthesis in vivo. *Annual Review of Plant Biology*, 59(1), 89– 113. https://doi.org/10.1146/annurev.arplant.59.032607.092759

Baldocchi, D., Falge, E., Gu, L., Olson, R., Hollinger, D., Running, S., et al. (2001). FLUXNET: A new tool to study the temporal and spatial variability of ecosystem-scale carbon dioxide, water vapor, and energy flux densities. *Bulletin of the American Meteorological Society*, 82(11), 2415– 2434. https://doi.org/10.1175/1520-0477(2001)082%3C2415:FANTTS%3E2.3.CO;2

Croft, H., Chen, J. M., Luo, X., Bartlett, P., Chen, B., & Staebler, R. M. (2016). Leaf chlorophyll content as a proxy for leaf photosynthetic capacity. *Global Change Biology*, 23(9), 3513– 3524.

Curran, P. J. (1989). Remote sensing of foliar chemistry. *Remote Sensing of Environment*, 30(3), 271– 278. https://doi.org/10.1016/0034-4257(89)90069-2

Dash, J., & Curran, P. J. (2004). The MERIS terrestrial chlorophyll index. *International Journal of Remote Sensing*, 25(23), 5403– 5413. https://doi.org/10.1080/0143116042000274015

Demarty, J., Chevallier, F., Friend, A. D., Viovy, N., Piao, S. L., & Ciais, P. (2007). Assimilation of global MODIS leaf area index retrievals within a

terrestrial biosphere model. *Geophysical Research Letters*, 34, L15402. https://doi.org/10.1029/2007GL030014

Deming, W. E. (1943). *Statistical adjustment of data*. Oxford, England: Wiley.

Elsobky, N. M. (2015). *Variation and uncertainty in MERIS sensor land biophysical variables at global scale*. Southampton, UK: University of Southampton.

Field, C. B. (1991). Ecological scaling of carbon gain to stress and resource. In *Response of Plants to Multiple Stresses* (pp. 35– 65). San Diego, CA: Academic Press. https://doi.org/10.1016/B978-0-08-092483-0.50007-4

Frankenberg, C., Fisher, J. B., Worden, J., Badgley, G., Saatchi, S. S., Lee, J. E., et al. (2011). New global observations of the terrestrial carbon cycle from GOSAT: Patterns of plant fluorescence with gross primary productivity. *Geophysical Research Letters*, 38, L17706. https://doi.org/10.1029/2011GL048738

Friedl, M. A., Sulla-Menashe, D., Tan, B., Schneider, A., Ramankutty, N., Sibley, A., & Huang, X. M. (2010). MODIS Collection 5 global land cover: Algorithm refinements and characterization of new datasets. *Remote Sensing of Environment*, 114(1), 168– 182. https://doi.org/10.1016/j.rse.2009.08.016

Genty, B., Briantais, J. M., & Baker, N. R. (1989). The relationship between the quantum yield of photosynthetic electron transport and quenching of chlorophyll fluorescence. *Biochimica et Biophysica Acta - General Subjects*, 990(1), 87– 92. https://doi.org/10.1016/S0304-4165(89)80016-9

Gitelson, A. A., & Gamon, J. A. (2015). The need for a common basis for defining light-use efficiency: Implications for productivity estimation. *Remote Sensing of Environment*, 156, 196– 201. https://doi.org/10.1016/j.rse.2014.09.017

Goetz, S. J., & Prince, S. D. (1999). Modelling terrestrial carbon exchange and storage: Evidence and implications of functional convergence in light-use efficiency. In A. H. Fitter & D. Raffaelli (Eds.), *Advances in Ecological Research* (pp. 57– 92). San Diego, CA: Academic Press. https://doi.org/10.1016/S0065-2504(08)60029-X

Guanter, L., Zhang, Y., Jung, M., Joiner, J., Voigt, M., Berry, J. A., et al. (2014). Global and time-resolved monitoring of crop photosynthesis with chlorophyll fluorescence. *Proceedings of the National Academy of Sciences of the United States of America*, 111(14), E1327– E1333. https://doi.org/10.1073/pnas.1320008111

Guerschman, J. P., Hill, M. J., Renzullo, L. J., Barrett, D. J., Marks, A. S., & Botha, E. J. (2009). Estimating fractional cover of photosynthetic vegetation, non-photosynthetic vegetation and bare soil in the Australian tropical savanna region upscaling the EO-1 Hyperion and MODIS

sensors. *Remote Sensing of Environment*, 113(5), 928– 945. https://doi.org/10.1016/j.rse.2009.01.006

Hilker, T., Lyapustin, A. I., Tucker, C. J., Hall, F. G., Myneni, R. B., Wang, Y., et al. (2014). Vegetation dynamics and rainfall sensitivity of the Amazon. *Proceedings of the National Academy of Sciences of the United States of America*, 111(45), 16,041– 16,046. https://doi.org/10.1073/pnas.1404870111

Huete, A., Didan, K., Miura, T., Rodriguez, E. P., Gao, X., & Ferreira, L. G. (2002). Overview of the radiometric and biophysical performance of the MODIS vegetation indices. *Remote Sensing of Environment*, 83(1-2), 195– 213. https://doi.org/10.1016/S0034-4257(02)00096-2

Joiner, J., Guanter, L., Lindstrot, R., Voigt, M., Vasilkov, A. P., Middleton, E. M., et al. (2013). Global monitoring of terrestrial chlorophyll fluorescence from moderate-spectral-resolution near-infrared satellite measurements: Methodology, simulations, and application to GOME-2. *Atmospheric Measurement Techniques*, 6(10), 2803– 2823. https://doi.org/10.5194/amt-6-2803-2013

Joiner, J., Yoshida, Y., Vasilkov, A. P., Schaefer, K., Jung, M., Guanter, L., et al. (2014). The seasonal cycle of satellite chlorophyll fluorescence observations and its relationship to vegetation phenology and ecosystem atmosphere carbon exchange. *Remote Sensing of Environment*, 152, 375– 391. https://doi.org/10.1016/j.rse.2014.06.022

Kross, A., Seaquist, J. W., & Roulet, N. T. (2016). Light use efficiency of peatlands: Variability and suitability for modeling ecosystem production. *Remote Sensing of Environment*, 183, 239– 249. https://doi.org/10.1016/j.rse.2016.05.004

Li, Z. Q., & Guo, X. L. (2016). Remote sensing of terrestrial non-photosynthetic vegetation using hyperspectral, multispectral, SAR, and LiDAR data. *Progress in Physical Geography*, 40(2), 276– 304. https://doi.org/10.1177/0309133315582005

Liu, L., Guan, L., & Liu, X. (2017). Directly estimating diurnal changes in GPP for C3 and C4 crops using far-red Sun-induced chlorophyll fluorescence. *Agricultural and Forest Meteorology*, 232, 1– 9. https://doi.org/10.1016/j.agrformet.2016.06.014

Lyapustin, A. I., Wang, Y., Laszlo, I., Hilker, T., Hall, F. G., Sellers, P. J., et al. (2012). Multi-angle implementation of atmospheric correction for MODIS (MAIAC): 3. Atmospheric correction. *Remote Sensing of Environment*, 127, 385– 393. https://doi.org/10.1016/j.rse.2012.09.002

McCallum, I., Wagner, W., Schmullius, C., Shvidenko, A., Obersteiner, M., Fritz, S., & Nilsson, S. (2009). Satellite-based terrestrial production

efficiency modeling. *Carbon Balance and Management*, 4(1), 8. https://doi.org/10.1186/1750-0680-4-8

Mercado, L. M., Bellouin, N., Sitch, S., Boucher, O., Huntingford, C., Wild, M., & Cox, P. M. (2009). Impact of changes in diffuse radiation on the global land carbon
sink. *Nature*, 458(7241), 1014– 1017. https://doi.org/10.1038/nature07949

Monteith, J. L. (1972). Solar-radiation and productivity in tropical ecosystems. *Journal of Applied Ecology*, 9(3), 747– 766. https://doi.org/10.2307/2401901

Myneni, R. B., Hoffman, S., Knyazikhin, Y., Privette, J. L., Glassy, J., Tian, Y., et al. (2002). Global products of vegetation leaf area and fraction absorbed PAR from year one of MODIS data. *Remote Sensing of Environment*, 83(1– 2), 214– 231. https://doi.org/10.1016/S0034-4257(02)00074-3

Myneni, R., Knyazikhin, Y., & Park, T. (2015). MOD15A2H MODIS/Terra leaf area index/FPAR 8-day L4 Global 500m SIN Grid V006, NASA EOSDIS Land Processes DAAC. https://doi.org/10.5067/MODIS/MOD15A2H.006

Pastorello, G., Papale, D., Chu, H., Trotta, C., Agarwal, D., Canfora, E., et al. (2017). The FLUXNET2015 dataset: The longest record of global carbon, water, and energy fluxes is updated. *Eos, Transactions American Geophysical Union*. https://doi.org/10.1029/2017EO071597

Peng, Y., Gitelson, A. A., Keydan, G., Rundquist, D. C., & Moses, W. (2011). Remote estimation of gross primary production in maize and support for a new paradigm based on total crop chlorophyll content. *Remote Sensing of Environment*, 115(4), 978– 989. https://doi.org/10.1016/j.rse.2010.12.001

Porcar-Castell, A., Tyystjarvi, E., Atherton, J., van der Tol, C., Flexas, J., Pfundel, E. E., et al. (2014). Linking chlorophyll a fluorescence to photosynthesis for remote sensing applications: Mechanisms and challenges. *Journal of Experimental Botany*, 65(15), 4065– 4095. https://doi.org/10.1093/jxb/eru191

Potter, C. S., Randerson, J. T., Field, C. B., Matson, P. A., Vitousek, P. M., Mooney, H. A., & Klooster, S. A. (1993). Terrestrial ecosystem production—A process model-based on global satellite and surface data. *Global Biogeochemical Cycles*, 7(4), 811– 841. https://doi.org/10.1029/93GB02725

Rossini, M., Cogliati, S., Meroni, M., Migliavacca, M., Galvagno, M., Busetto, L., et al. (2012). Remote sensing-based estimation of gross primary production in a subalpine grassland. *Biogeosciences*, 9(7), 2565– 2584. https://doi.org/10.5194/bg-9-2565-2012

Running, S. W., Nemani, R. R., Heinsch, F. A., Zhao, M. S., Reeves, M., & Hashimoto, H. (2004). A continuous satellite-derived measure of global terrestrial primary

production. *Bioscience*, 54(6), 547– 560. https://doi.org/10.1641/0006-3568(2004)054%5B0547:ACSMOG%5D2.0.CO;2

Song, C. H., Dannenberg, M. P., & Hwang, T. (2013). Optical remote sensing of terrestrial ecosystem primary productivity. *Progress in Physical Geography*, 37(6), 834– 854. https://doi.org/10.1177/0309133313507944

Sun, Y., Frankenberg, C., Wood, J. D., Schimel, D. S., Jung, M., Guanter, L., et al. (2017). OCO-2 advances photosynthesis observation from space via solar-induced chlorophyll
fluorescence. *Science*, 358(6360), 189. https://doi.org/10.1126/science.aam5747

van der Tol, C., Berry, J. A., Campbell, P. K. E., & Rascher, U. (2014). Models of fluorescence and photosynthesis for interpreting measurements of solar-induced chlorophyll fluorescence. *Journal of Geophysical Research: Biogeosciences*, 119, 2312– 2327. https://doi.org/10.1002/2014JG002713

van der Tol, C., Verhoef, W., & Rosema, A. (2009). A model for chlorophyll fluorescence and photosynthesis at leaf scale. *Agricultural and Forest Meteorology*, 149(1), 96– 105.

van der Tol, C., Verhoef, W., Timmermans, J., Verhoef, A., & Su, Z. (2009). An integrated model of soil-canopy spectral radiances, photosynthesis, fluorescence, temperature and energy
balance. *Biogeosciences*, 6(12), 3109– 3129.

Verhoef, W. (1984). Light-scattering by leaf layers with application to canopy reflectance modeling—The sail model. *Remote Sensing of Environment*, 16(2), 125– 141. https://doi.org/10.1016/0034-4257(84)90057-9

Verhoef, W. (2011). Modelling vegetation fluorescence observations, edited, ARSel Proceedings of the 7th SIG-imaging Spectroscopy Workshop.

Vermote, E. F. (2015). MOD09A1 MODIS surface reflectance 8-day L3 Global 500m SIN Grid V006, NASA EOSDIS Land Processes DAAC.

Verrelst, J., Rivera, J. P., van der Tol, C., Magnani, F., Mohammed, G., & Moreno, J. (2015). Global sensitivity analysis of the SCOPE model: What drives simulated canopy-leaving Sun-induced fluorescence? *Remote Sensing of Environment*, 166, 8– 21. https://doi.org/10.1016/j.rse.2015.06.002

Viovy, N., Arino, O., & Belward, A. (1992). The Best Index Slope Extraction (BISE): A method for reducing noise in NDVI time-series. *International Journal of Remote
Sensing*, 13(8), 1585– 1590. https://doi.org/10.1080/01431169208904212

Wu, J., Albert, L. P., Lopes, A. P., Restrepo-Coupe, N., Hayek, M., Wiedemann, K. T., et al. (2016). Leaf development and demography explain photosynthetic seasonality in Amazon evergreen
forests. *Science*, 351(6276), 972– 976.

Xiao, X., Zhang, Q., Braswell, B., Urbanski, S., Boles, S., Wofsy, S., et al. (2004). Modeling gross primary production of temperate deciduous broadleaf forest using satellite images and climate data. *Remote Sensing of Environment*, 91(2), 256– 270. https://doi.org/10.1016/j.rse.2004.03.010

Yan, K., Park, T., Yan, G., Liu, Z., Yang, B., Chen, C., et al. (2016). Evaluation of MODIS LAI/FPAR Product Collection 6. Part 2: Validation and intercomparison. *Remote Sensing*, 8(6), 460. https://doi.org/10.3390/rs8060460

Yang, X., Tang, J., Mustard, J. F., Lee, J.-E., Rossini, M., Joiner, J., et al. (2015). Solar-induced chlorophyll fluorescence correlates with canopy photosynthesis on diurnal and seasonal scales in a temperate deciduous forest. *Geophysical Research Letters*, 42, 2977– 2987. https://doi.org/10.1002/2015GL063201

Zhang, Y., Guanter, L., Berry, J. A., Joiner, J., van der Tol, C., Huete, A., et al. (2014). Estimation of vegetation photosynthetic capacity from space-based measurements of chlorophyll fluorescence for terrestrial biosphere models. *Global Change Biology*, 20(12), 3727– 3742. https://doi.org/10.1111/gcb.12664

Zhang, Q. Y., Middleton, E. M., Margolis, H. A., Drolet, G. G., Barr, A. A., & Black, T. A. (2009). Can a satellite-derived estimate of the fraction of PAR absorbed by chlorophyll (FAPAR(chl)) improve predictions of light-use efficiency and ecosystem photosynthesis for a boreal aspen forest? *Remote Sensing of Environment*, 113(4), 880– 888. https://doi.org/10.1016/j.rse.2009.01.002

Zhang, Y., Xiao, X., Jin, C., Dong, J., Zhou, S., Wagle, P., et al. (2016). Consistency between Sun-induced chlorophyll fluorescence and gross primary production of vegetation in North America. *Remote Sensing of Environment*, 183, 154– 169. https://doi.org/10.1016/j.rse.2016.05.015

Zhang, Y., Xiao, X., Wu, X., Zhou, S., Zhang, G., Qin, Y., & Dong, J. (2017). A global moderate resolution dataset of gross primary production of vegetation for 2000–2016. *Scientific Data*, 4, 170165. https://doi.org/10.1038/sdata.2017.165

Zhang, Y., Xiao, X., Zhou, S., Ciais, P., McCarthy, H., & Luo, Y. (2016). Canopy and physiological controls of GPP during drought and heat wave. *Geophysical Research Letters*, 43, 3325– 3333. https://doi.org/10.1002/2016GL068501

Zhao, M., Heinsch, F. A., Nemani, R. R., & Running, S. W. (2005). Improvements of the MODIS terrestrial gross and net primary production global data set. *Remote Sensing of Environment*, 95(2), 164– 176. https://doi.org/10.1016/j.rse.2004.12.011